Rapid Communications

Unconventional superconductivity in a doped quantum spin Hall insulator

Xianxin Wu, Mario Fink, Werner Hanke, Ronny Thomale, and Domenico Di Sante*
Institut für Theoretische Physik und Astrophysik, Universität Würzburg, Am Hubland Campus Süd, Würzburg 97074, Germany

(Received 15 November 2018; published 31 July 2019)

A monolayer of jacutingaite (Pt_2HgSe_3) has recently been identified as a novel quantum spin Hall insulator. By first-principles calculations, we study its Fermiology in the doped regime and unveil a type-I and type-II van Hove singularity for hole and electron doping, respectively. We find that the common link between the propensity for a topological band gap at pristine filling and unconventional superconductivity at finite doping is rooted in the longer-ranged hybridization integrals on the honeycomb lattice. In a combined effort of random phase approximation and functional renormalization group, we find chiral d-wave order for the type-I and odd-parity f-wave order for the type-II regime. When longer-ranged Coulomb interaction is included, a propensity of the type-II regime towards a topological $p_x + ip_y$-wave order emerges.

DOI: 10.1103/PhysRevB.100.041117

Introduction. The quantum spin Hall (QSH) effect and unconventional superconductivity are among the most intensely studied fields of contemporary condensed matter research [1–3]. At a superficial level, both topical areas do not seem to be particularly intertwined: In the pursuit of a quantum spin Hall insulator with the most preferable properties, essential parameters of optimization include spin-orbit coupling and other single-particle properties to enhance the topological bulk gap; in order to accomplish a high-T_c unconventional superconductor as a quantum many-body state of matter, tuning the electronic interaction strength and profile appears as the most relevant guiding principle.

Still, superconductivity and topological band insulators or semimetals have previously faced each other in several contexts. Most prominently, this holds for the principal topological classification of single-particle scenarios where the emergent particle-hole symmetry in superconductors plays a pivotal role [4], and for the case of the superconducting proximity effect imposed on a topologically nontrivial band structure [5–8]. All these instances, however, do not include the joint avenue of a superconductor and a topological band insulator in the same material at only different doping. Ideally, such a setting might allow for the synthesis of a high-quality domain boundary between a superconductor and a topological insulator with identical lattice structures, under the assumption that it were possible to impose distinct gating in both domains. Until today, there are only a few reports of materials that are believed to be both topological insulators and superconductors. Half-Heusler semimetals [9], Cu-doped Bi_2Se_3 [10], doped $BaBiO_3$ [11,12], and monolayer WTe_2 [13] are such remarkable exceptions, where a conventional, i.e., phonon-driven, mechanism for superconductivity is likely to dominate.

In this Rapid Communication, we propose a monolayer of jacutingaite (Pt_2HgSe_3) to host, besides a quantum spin Hall insulator at pristine filling [14,15], different phases of unconventional superconductivity for finite hole and electron doping. The central overarching motif that enables both the realization of the quantum spin Hall effect and unconventional superconductivity is a specific longer-ranged hybridization profile which is rooted in the extended Wannier functions of jacutingaite (Fig. 1). The multiorbital composition and the honeycomb monolayer buckling conspire to yield an effective tight-binding description which not only provides for a large topological band gap, but also gives rise to van Hove singularities (vHs) close by pristine filling, with a type-I profile for the hole and type-II profile for electron doping. For type I, the saddle points locate at the time-reversal invariant momenta (TRIM) **M** of the hexagonal lattice. For type II, the saddle points appear along the **K**-**M** lines in the Brillouin zone, and hence do not coincide with TRIM [16,17]. As such, while the van Hove induced enhancement of the Fermi level density of states promotes unconventional superconductivity in general, the nature of the unconventional superconducting state sensitively depends on the type-I versus type-II regime, which we analyze through the random phase approximation (RPA) and functional renormalization group (FRG). We find a d-wave instability for the type-I setting which yields spontaneous time-reversal symmetry breaking according to a chiral d-wave state. For the type-II setting, the ferromagnetic fluctuations dominate and promote a competition between an odd-parity f-wave and a topological $p_x + ip_y$-wave state upon changes in the long-range character of the Coulomb interaction.

Effective model. Monolayer jacutingaite crystallizes in the space group $P\bar{3}m1$ (No. 164), where the Hg atoms form a buckled honeycomb lattice surrounded by triangles of Pt and Se [Fig. 1(a)]. As first pointed out by Marrazzo *et al.* [14], the low-energy band structure of jacutingaite can be reduced to an effective tight-binding description that shares several terms with the Kane-Mele model for a quantum spin Hall insulator in graphene [1]. Anticipating its relevance for jacutingaite at finite doping, we further add hybridization integrals up to

*domenico.disante@physik.uni-wuerzburg.de

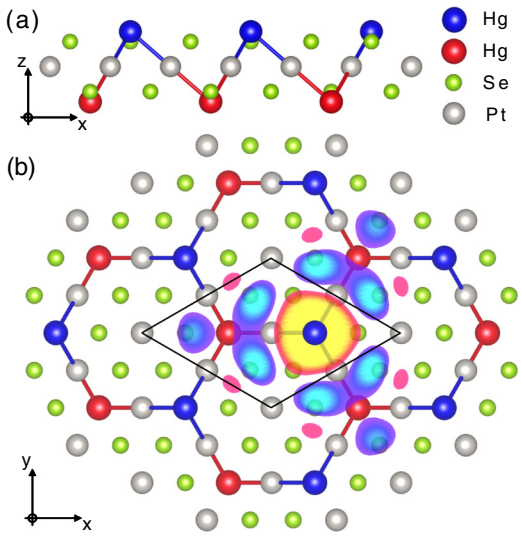

FIG. 1. (a) Side and (b) top views of the Pt_2HgSe_3 crystal structure. In (b), a representation of the Wannier function whose in-plane center of mass coincides with the top Hg is shown. Yellow and blue refer to positive and negative values of the Wannier function. The Wannier function originating from the bottom Hg can be obtained by inversion.

fourth-nearest neighbor which yields

$$H_0^{\mathrm{J}} = \sum_{n=1}^{4} t_n \sum_{\langle ij\rangle_n} c_i^\dagger c_j + i\lambda_{\mathrm{SO}} \sum_{\langle ij\rangle_2} \nu_{ij} c_i^\dagger \sigma^z c_j + i\lambda_{\mathrm{R}} \sum_{\langle ij\rangle_2} \mu_{ij} c_i^\dagger (\boldsymbol{\sigma} \times \hat{\mathbf{d}}_{ij})_z c_j. \quad (1)$$

Such a long-range hybridization character originates from the delocalized nature of Hg 6*s* and Pt 5*d* orbitals, which mix to form the hermaphrodite Wannier functions shown in Fig. 1(b).

The parameters t_n, λ_{SO}, and λ_{R} are real, where t_n denotes the nth nearest-neighbor hopping, λ_{SO} is the spin-orbit coupling (SOC) induced second-nearest-neighbor hopping, and λ_{R} describes the Rashba SOC. The absence of a Semenoff mass is due to the centrosymmetric structure of jacutingaite, i.e., the two Wannier functions composing the low-energy model have the same on-site energy. The imaginary parts of nearest- and third-nearest-neighbor hopping vanish due to mirror (with respect to the Hg-Hg bonds) and time-reversal symmetries. Note that t_2 connects equal sublattices on the honeycomb lattice, and as such breaks the chiral symmetry. The chiral symmetry operator is $S = \sum_i c_{is}^\dagger \tau_{z,ss'} c_{is'}$, where $s(s')$ represents the sublattice index. Since $S^{-1} H_0^{\mathrm{J}} S \neq -H_0^{\mathrm{J}}$ when a real t_2 hopping is included, the resulting energy spectrum ceases to be chiral symmetric in the presence of finite t_2. The parameters extracted by projecting the density functional theory Hamiltonian onto a set of maximally localized Wannier orbitals at different levels of sophistication [18], as shown in Fig. 2(a) for the Heyd-Scuseria-Ernzerhof (HSE)(+SOC) cases, are summarized in Table I.

TABLE I. Model parameters extracted by projecting the low-energy states onto two hermaphrodite Wannier orbitals, that map onto each other under inversion. One of the two is shown in Fig. 1(b). All the parameters are given in meV. Only hopping terms up to the fourth-nearest-neighbor t_4 are shown. (PBE=Perdew-Burke-Ernzerhof).

	t_1	t_2	λ_{SO}	λ_{R}	t_3	t_4
PBE+SOC	168	−25	18	28	11	−16
HSE+SOC	265	−28	21	27	−0.4	−28
PBE	178	−31			16	−24
HSE	267	−35			4	−32

The topological bulk gap yields $E_g \sim 6\sqrt{3}\lambda_{\mathrm{SO}}$. Note that λ_{SO} in a Kane-Mele single-orbital scenario describes an effective SOC which, starting from the local atomic term, also considers a downscaling due to the higher-order perturbative effect via second-nearest-neighbor hybridization. In a QSH material candidate such as graphene, this leads to a significant reduction of λ_{SO} because the longer-range hybridization is small [19], whereas for jacutingaite, this rescaling is much weaker, combined with the enhanced atomic SOC of Hg in comparison to C. An alternative path to enhance E_g is to realize a two-orbital model per site, as such allowing for local atomic SOC to affect the low-energy effective model and to avoid the rescaling due to longer-range hybridization. This is accomplished for bismuthene on SiC [20,21].

Aside from the large gap, further relevant aspects of the resulting band structure are visible as we analyze the precise

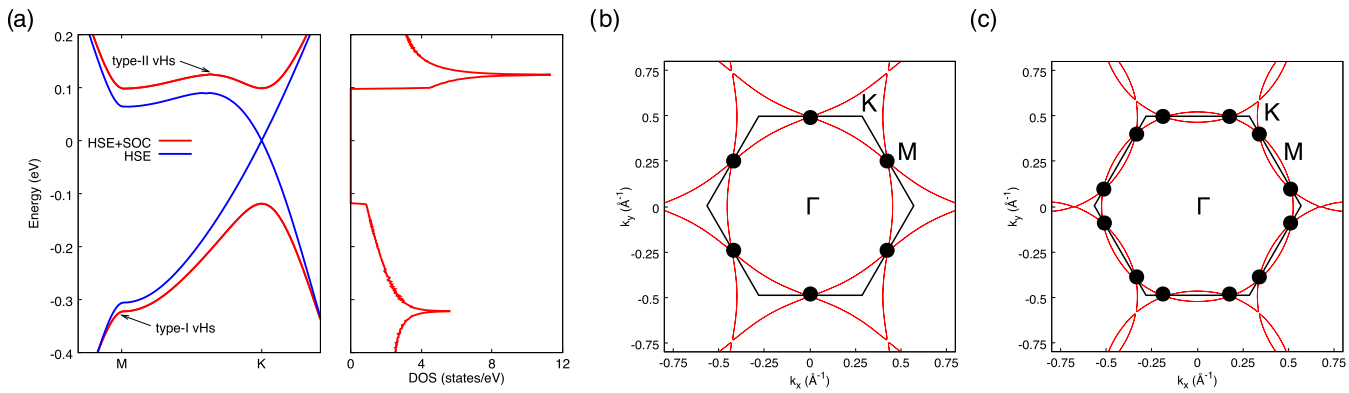

FIG. 2. (a) Low-energy band structure of Pt_2HgSe_3 at the HSE(+SOC) level of accuracy. The right panel shows the density of states (DOS) for the calculation including SOC. (b), (c) Fermi surface at the type-I and type-II vHs, respectively. The black dots highlight the saddle points where the DOS diverges logarithmically.

dispersion of the bands in the two-dimensional Brillouin zone. By looking at the DOS in Fig. 2(a), vHs peaks arise at the **M** point for the valence band and along the **K**-**M** line for the conduction band, respectively. The Fermi surface at the former vHs [Fig. 2(b)] shows a hexagonal profile, with triangular hole pockets around the **K** points. The Fermi surface at the latter vHs [Fig. 2(c)], on the other hand, shows a different shape, with small pockets touching at the saddle points. We refer to this vHs as type II [16,17], to distinguish it from the type-I vHs where the saddle points locate at TRIM. A necessary condition for a coexistence of both type-I and type-II vHs in jacutingaite is a sizable real hopping parameter t_2 in (1). This contribution is not contained in the Kane-Mele model [1], but indispensable to account for a realistic setting such as the buckled honeycomb lattice of monolayer jacutingaite. To reproduce the band dispersion given by first-principles calculations, and in particular to obtain the type-II vHs we find in jacutingaite, longer-range hoppings t_3 and t_4 need to be taken into consideration (Table I). While those new terms do not change the principal topological nature of the bulk band gap [14], they are of primary importance for an accurate study of pairing states nearby van Hove filling [18].

Superconducting instabilities. In order to account for electronic interactions, we consider the on-site Hubbard model on the 2D hexagonal lattice, with the noninteracting single-particle Hamiltonian given by (1), and U parametrizing the Hubbard coupling strength. The full Hamiltonian reads

$$H^{\mathrm{J}} = H_0^{\mathrm{J}} + U\sum_i n_{i\uparrow}n_{i\downarrow} - \mu\sum_{i,\sigma} n_{i,\sigma}, \tag{2}$$

where μ is the chemical potential tuned to access the two vH regimes. The combination of Fermi level density of states and finite U triggers superconducting instabilities, which we analyze in the following. At the simplified RPA level, where the electronic two-particle vertex function is replaced by the bare interaction U, an effective attractive interaction can emerge through the exchange of charge and magnetic fluctuations. These are governed by the respective charge and magnetic susceptibilities $\chi^{\mathrm{ph}}_{c/m}(\mathbf{q}) = [1 \pm U\chi^{\mathrm{ph}}_0(\mathbf{q})]^{-1}\chi^{\mathrm{ph}}_0(\mathbf{q})$. The zero-frequency component of the bare susceptibility matrix in the particle-hole channel is defined as

$$\left[\chi^{\mathrm{ph}}_0(\mathbf{q})\right]^{l_1 l_3}_{l_2 l_4} = -\frac{1}{N_k}\sum_{\mathbf{k},nm} a_n^{l_2}(\mathbf{k})a_n^{l_4*}(\mathbf{k})a_m^{l_3}(\mathbf{k}+\mathbf{q}) \times a_m^{l_1*}(\mathbf{k}+\mathbf{q})\frac{f(\varepsilon_{n\mathbf{k}}) - f(\varepsilon_{m\mathbf{k}+\mathbf{q}})}{\varepsilon_{n\mathbf{k}} - \varepsilon_{m\mathbf{k}+\mathbf{q}}}, \tag{3}$$

where $l_i = 1, 2$ is the sublattice index and $a_n^{l_i}(\mathbf{k})$ is the l_ith component of the nth eigenvector. This quantity reveals the distribution of momentum transfer $\mathbf{q}$ implied by spin and charge fluctuations.

In Fig. 3(a) we show the susceptibility $\chi^{\mathrm{ph}}_0(\mathbf{q})$ at the type-I vHs. A significant intensity close to the **M** point suggests dominant antiferromagnetic spin fluctuations in the system, and is a consequence of the high degree of nesting of the Fermi surface at the type-I vHs, as evident from Fig. 2(b). Such a setting for spin fluctuations has been found to trigger an even-parity chiral superconducting instability [22–24]. At the type-II vHs, on the other hand, there is no Fermi surface

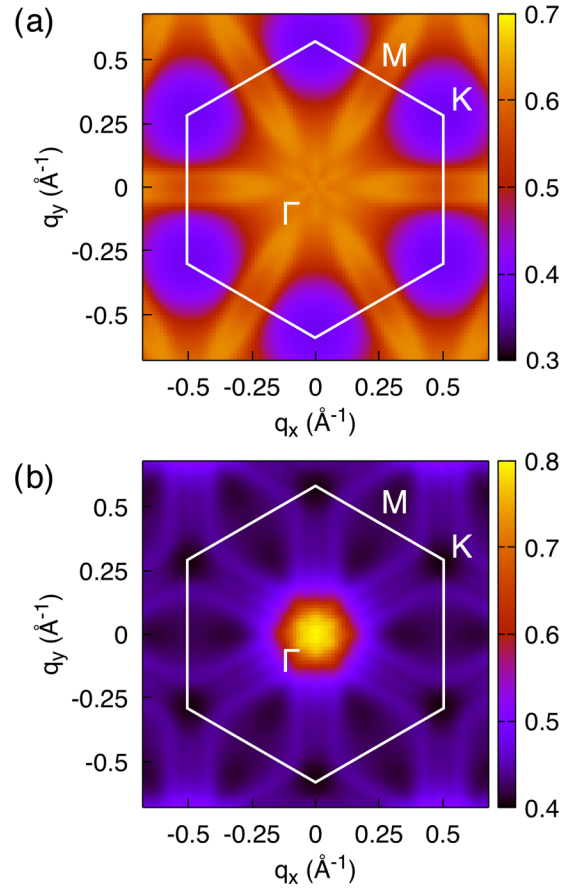

FIG. 3. Distribution of the bare particle-hole susceptibility $\chi^{\mathrm{ph}}_0(\mathbf{q}) = \frac{1}{2}\sum_{l_1 l_2}[\chi^{\mathrm{ph}}_0(\mathbf{q})]^{l_1 l_2}_{l_1 l_2}$ (at the HSE level) at the (a) type-I vHs and (b) type-II vHs, respectively.

nesting, and $\chi^{\mathrm{ph}}_0(\mathbf{q})$ is solely peaked around the $\mathbf{\Gamma}$ point, suggesting that in this case, the dominant magnetic fluctuations involve a long-range modulation (i.e., ferromagnetic fluctuations in the limit $\mathbf{q} \to \mathbf{0}$). General arguments based on analytical weak-coupling renormalization group applied to saddle points located not at TRIM, close to type-II vHs, point to a spin-triplet odd-parity superconducting state [16,17].

In order to provide a most substantiated analysis of the superconducting instabilities, we apply a combined effort of RPA and FRG. For the problem at hand, we find that all approaches we have used reach the same conclusion on the nature of the superconducting state. Since the FRG tracks vertex corrections and treats all instability channels on equal footing, we choose to discuss the FRG results in the main text, and defer the confirming evidence from RPA to the Supplemental Material [18]. Within FRG, we formulate a set of coupled integrodifferential equations which describes a two-particle vertex flow equation V_Λ where the temperature flow parameter Λ corresponds to the cutoff parameter that evolves from high energies towards the Fermi level [25,26]. Within the patch-FRG we employ here, the two-particle vertex is projected to the Fermi level, and discretized into $N = 96$ patches. The initial condition for the $96^3 \sim 8.8 \times 10^5$-dimensional system of integrodifferential equations is given by the many-body interaction U. In order to further improve the numerical performance, we consider the HSE *ab initio*

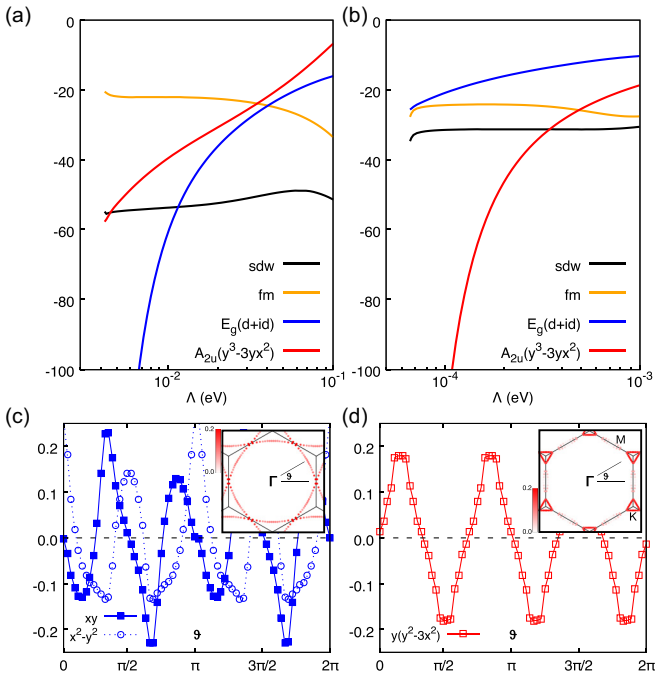

FIG. 4. FRG flow for monolayer jacutingaite at the (a) type-I vHs and (b) type-II vHs ($U = 2.5$). (c) and (d) show the form factors along the Fermi surface for the leading superconducting instabilities found in (a) and (b), respectively. The insets in (c) and (d) report the gap function along the Fermi surface from a subsequent treatment of the leading FRG instabilities in mean-field theory.

band structure without SOC in order to exploit full SU(2) symmetry, and obtain the spin triplet and singlet sectors by vertex antisymmetrization and symmetrization, respectively. This approximation is justified for the case of jacutingaite. As already hinted at in Fig. 2(a) and carefully checked by us, the SOC term predominantly serves to open a band gap, but hardly affects the Fermi surface dispersion and eigenstates at the electron- and hole-doped van Hove levels. A minor difference is given for the precise location of the saddle points along the **K**-**M** lines for the type-II vHs, or the degree of warping for the type-I vHs. Facing the choice between enhanced radial resolution via more patches and tracking those minor differences in terms of SOC-inclusive Fermiology, we find it preferable to keep maximal radial resolution.

Within FRG, the renormalized interaction V_Λ starts to diverge in some channel as the infrared cutoff Λ approaches the Fermi surface; this marks the onset of a leading instability, which we subsequently analyze within mean-field theory [27]. The FRG procedure adjusted to the Fermi surface instabilities of interacting fermions allows for an equal treatment of all possible two-particle instabilities, which is an immediate advantage in comparison to RPA where the procedure is constrained to only a single two-particle channel of interest, such as particle-particle or particle-hole. While the precise validity range of FRG in terms of interaction strength still cannot be rigorously specified, it provides numerical guidance to model interacting electron systems at intermediate coupling.

Figure 4(a) shows that when the chemical potential locates nearby the type-I vHs, the effective interaction V_Λ diverges in the even-parity spin-singlet superconducting channel. Its two degenerate order parameters d_{xy} and $d_{x^2-y^2}$ transform as the two-dimensional E_g irreducible representation of D_{3d}, the point group of the buckled honeycomb structure. The gap functions $\Delta_{d_{xy}}$ and $\Delta_{d_{x^2-y^2}}$ both have line nodes along the Fermi surface [form factors depicted in Fig. 4(c)]. As evident from a subsequent mean-field treatment, the system gains condensation energy below the instability level by removing the nodes via complex superposition $d_{xy} \pm i d_{x^2-y^2}$ [inset of Fig. 4(c)], a manifestation of spontaneous time-reversal symmetry breaking. As a subleading pairing channel, f-wave pairing emerges, which is also observed within RPA [18].

When the chemical potential is shifted to the type-II vHs, the Fermi surface is dominated by ferromagnetic fluctuations, which favors a superconducting instability in the spin-triplet sector [Fig. 4(b)]. The form factor of the leading instability transforms according to the one-dimensional A_{2u} irreducible representation of D_{3d}, i.e., the superconducting state resides in the $f_{y(3x^2-y^2)}$-wave state [Fig. 4(d)]. Again, RPA calculations are consistent with FRG in this setting [18].

Ultimately, for a underlying electronic structure as in jacutingaite, where the longer ranged hoppings play an important role, nonlocal Coulomb repulsions besides the Hubbard on-site term can be pivotal for determining the correct symmetry of the SC pairing state [28]. In the Supplemental Material [18] we show indeed that the p-wave pairing can eventually dominate over the f-wave state when terms beyond the on-site interaction are considered. The degenerate p_x and p_y order parameters transform as the two-dimensional E_u irreducible representation of D_{3d}, and as such, the system tends to favor a topological $p_x + ip_y$-wave superposition to gain the maximum in condensation energy [18]. This unconventional pairing can also host Majorana bound states. Experimental signatures that distinguish between the different paring symmetries can be obtained by the analysis of the scanning tunneling microscopy (STM) differential conductance spectra (dI/dV) [29].

Conclusions. We have identified monolayer jacutingaite as a promising host not only for a quantum spin Hall phase at pristine filling [14,15,30], but also for unconventional superconductivity at van Hove filling for electron and hole doping. The type-I vHs is reached upon doping by 0.39 holes, which corresponds to about 9.8% hole doping. For the type-II vHs, even only 4.0% electron doping (~0.16 electrons) is needed, a value that in principle may even already be achieved by electrolytic gating. In addition to the interest generated due to its inherently exotic nature, the high experimental feasibility of possibly accomplishing a type-II van Hove level without chemical doping is a highly appealing feature of monolayer jacutingaite. Note that, for instance, several attempts were made to dope graphene to the vHs point by Ca and K adsorbates [31]. Notwithstanding the efforts, so far no evidence of superconductivity was reported. Conversely, the rather small amount of doping needed to reach the type-II vHs renders jacutingaite a promising material candidate to realistically achieve unconventional superconductivity in a doped quantum spin Hall insulator.

Acknowledgments. We thank A. Marrazzo and G. Sangiovanni for discussions. This work was funded by the

Deutsche Forschungsgemeinschaft (DFG, German Research Foundation) – Project-ID 258499086 – SFB 1170 (Project B06) and by the Dresden-Würzburg Center for Topological Quantum Matter Research (ct.qmat). We gratefully acknowledge the Gauss Centre for Supercomputing e.V. [38] for funding this project by providing computing time on the GCS Supercomputer SuperMUC at Leibniz Supercomputing Centre [39].

[1] C. L. Kane and E. J. Mele, Phys. Rev. Lett. **95**, 146802 (2005).
[2] B. A. Bernevig, T. L. Hughes, and S.-C. Zhang, Science **314**, 1757 (2006).
[3] M. Sigrist and K. Ueda, Rev. Mod. Phys. **63**, 239 (1991).
[4] A. P. Schnyder, S. Ryu, A. Furusaki, and A. W. W. Ludwig, Phys. Rev. B **78**, 195125 (2008).
[5] L. Fu and C. L. Kane, Phys. Rev. Lett. **100**, 096407 (2008).
[6] J. D. Sau, R. M. Lutchyn, S. Tewari, and S. Das Sarma, Phys. Rev. Lett. **104**, 040502 (2010).
[7] R. M. Lutchyn, J. D. Sau, and S. Das Sarma, Phys. Rev. Lett. **105**, 077001 (2010).
[8] Y. Oreg, G. Refael, and F. von Oppen, Phys. Rev. Lett. **105**, 177002 (2010).
[9] Y. Nakajima, R. Hu, K. Kirshenbaum, A. Hughes, P. Syers, X. Wang, K. Wang, R. Wang, S. R. Saha, D. Pratt, J. W. Lynn, and J. Paglione, Sci. Adv. **1**, e1500242 (2015).
[10] Y. S. Hor, A. J. Williams, J. G. Checkelsky, P. Roushan, J. Seo, Q. Xu, H. W. Zandbergen, A. Yazdani, N. P. Ong, and R. J. Cava, Phys. Rev. Lett. **104**, 057001 (2010).
[11] B. Yan, M. Jansen, and C. Felser, Nat. Phys. **9**, 709 (2013).
[12] G. Li, B. Yan, R. Thomale, and W. Hanke, Sci. Rep. **5**, 10435 (2015).
[13] V. Fatemi, S. Wu, Y. Cao, L. Bretheau, Q. D. Gibson, K. Watanabe, T. Taniguchi, R. J. Cava, and P. Jarillo-Herrero, Science **362**, 926 (2018).
[14] A. Marrazzo, M. Gibertini, D. Campi, N. Mounet, and N. Marzari, Phys. Rev. Lett. **120**, 117701 (2018).
[15] K. Kandrai, G. Kukucska, P. Vancsó, J. Koltai, G. Baranka, Z. E. Horváth, Á. Hoffmann, A. Vymazalová, L. Tapasztó, and P. Nemes-Incze, arXiv:1903.02458.
[16] H. Yao and F. Yang, Phys. Rev. B **92**, 035132 (2015).
[17] Z. Y. Meng, F. Yang, K.-S. Chen, H. Yao, and H.-Y. Kee, Phys. Rev. B **91**, 184509 (2015).
[18] See Supplemental Material at http://link.aps.org/supplemental/10.1103/PhysRevB.100.041117 for details on the tight-binding model, as well as RPA and first-principles DFT calculations, which includes Refs. [32–37].
[19] C.-C. Liu, H. Jiang, and Y. Yao, Phys. Rev. B **84**, 195430 (2011).
[20] F. Reis, G. Li, L. Dudy, M. Bauernfeind, S. Glass, W. Hanke, R. Thomale, J. Schäfer, and R. Claessen, Science **357**, 287 (2017).
[21] G. Li, W. Hanke, E. M. Hankiewicz, F. Reis, J. Schäfer, R. Claessen, C. Wu, and R. Thomale, Phys. Rev. B **98**, 165146 (2018).
[22] R. Nandkishore, L. S. Levitov, and A. V. Chubukov, Nat. Phys. **8**, 158 (2012).
[23] W.-S. Wang, Y.-Y. Xiang, Q.-H. Wang, F. Wang, F. Yang, and D.-H. Lee, Phys. Rev. B **85**, 035414 (2012).
[24] M. L. Kiesel, C. Platt, W. Hanke, D. A. Abanin, and R. Thomale, Phys. Rev. B **86**, 020507(R) (2012).
[25] W. Metzner, M. Salmhofer, C. Honerkamp, V. Meden, and K. Schönhammer, Rev. Mod. Phys. **84**, 299 (2012).
[26] C. Platt, W. Hanke, and R. Thomale, Adv. Phys. **62**, 453 (2013).
[27] J. Reiss, D. Rohe, and W. Metzner, Phys. Rev. B **75**, 075110 (2007).
[28] C. Honerkamp, Phys. Rev. Lett. **100**, 146404 (2008).
[29] L. Elster, C. Platt, R. Thomale, W. Hanke, and E. M. Hankiewicz, Nat. Commun. **6**, 8232 (2015).
[30] J. I. Facio, S. K. Das, Y. Zhang, K. Koepernik, J. van den Brink, and I. C. Fulga, arXiv:1903.05001.
[31] J. L. McChesney, A. Bostwick, T. Ohta, T. Seyller, K. Horn, J. González, and E. Rotenberg, Phys. Rev. Lett. **104**, 136803 (2010).
[32] G. Kresse and J. Furthmüller, Phys. Rev. B **54**, 11169 (1996).
[33] J. P. Perdew, K. Burke, and M. Ernzerhof, Phys. Rev. Lett. **77**, 3865 (1996).
[34] J. Heyd, G. E. Scuseria, and M. Ernzerhof, J. Chem. Phys. **121**, 1187 (2004).
[35] A. A. Mostofi, J. R. Yates, Y.-S. Lee, I. Souza, D. Vanderbilt, and N. Marzari, Comput. Phys. Commun. **178**, 685 (2008).
[36] N. E. Bickers, D. J. Scalapino, and S. R. White, Phys. Rev. Lett. **62**, 961 (1989).
[37] S. Graser, T. A. Maier, P. J. Hirschfeld, and D. J. Scalapino, New J. Phys. **11**, 025016 (2009).
[38] http://www.gauss-centre.eu
[39] http://www.lrz.de